Full-Wave Analysis of Loaded Dipole Antennas using Mode-Matching Theory

Amir Jafargholi and Manouchehr Kamyab

Department of Electrical Engineering
K. N. Toosi University of Technology, P.O.Box 16315-1355. Tehran, Iran
Jafargholi@ee.kntu.ac.ir, Kamyab@kntu.ac.ir

Abstract **─** The influence of the material inclusions on the input impedance of the loaded dipoles excited by a delta function is analytically investigated. Novel and accurate analytical expressions for the input impedance of the loaded dipoles are proposed based on the mode matching technique. The boundary conditions are also enforced to obtain several simultaneous equations for the discrete modal coefficients inside the radiating region. Study of the input impedance of the whole multilayered structure is accomplished by the cascade connection of mediums as characterized by their constitutive parameters. The derived formulas are successfully validated through a proper comparison with the results obtained with the commercial software CST Microwave Studio.

Index Terms **─** Loaded dipole, mode-matching.

I. INTRODUCTION

In recent years, the introduction of metamaterials (MTMs) opened the way for many research groups to enhance antenna performances. Due to unique electromagnetic properties, MTMs have been widely considered in monopole and dipole antennas to improve their performance [1-5]. The problem of dielectric loaded wire antenna is heretofore analyzed using numerical methods, e.g., method of moment (MoM) [6], finite difference time domain (FDTD) [7], and simulations based on commercial software [8]. However, the analytical analysis of the dielectric loaded dipole antennas has not been reported in the literature.

The novelty of this paper is to introduce a mode-matching analysis of a dipole antenna loaded with material inclusions. The concept of the MTM loaded dipole is very important and, as to the authors' best knowledge, there are no papers reporting analytical expressions and full-wave analysis of this class of loaded antennas. In this paper, a theoretical formulation for a multiply dielectric loaded slotted spherical antenna is proposed based on the mode-matching method, to predict the behavior of the loaded dipole. It is worth noting that the radiation pattern of a finite length small angle biconical antenna differs only slightly from the pattern of a dipole [9]. Here, since the biconical antenna can be exactly analyzed and it also reduces, in the limiting case, to a cylindrical dipole antenna [10], this structure is considered for the analytical investigations. The obtained analytical formulas confirm the general conclusions recently presented in [7, 8], regarding the effect of material inclusions on the dipole antenna performance. It is demonstrated that the inclusion influence on the input impedance of a dipole is significant only for double-negative (DNG) MTM inclusions. The analytical results have been successfully validated through a comparison with the numerical results. The CST MICROWAVE is adopted for the simulations.

II. FIELD ANALYSIS

Figure 1a, illustrates a slotted dielectric loaded hollow conducting sphere of radius a, containing a Hertzian dipole $\bar{J} = \hat{z}J\delta(\bar{r} - \bar{r}')$, placed at the center ($r = r', \theta = 0, \varphi$), here (r, θ, φ) are the spherical coordinates and δ is a delta function. The time convention is $e^{-j\omega t}$ suppressed throughout. Due to

Submitted On: Aug. 15, 2011
Accepted On: Dec. 18, 2011

azimuthally symmetry, the fields depend on (r,θ) and the fields are then TM waves, which can be expressed in terms of magnetic vector potentials. The total magnetic vector potential for the un-slotted sphere (First region, I) is a sum of the primary and secondary magnetic vector potentials, [11].

$$A^i(r,\theta)=\hat{z}A_z^p(r,\theta)+\hat{r}A_r^s(r,\theta), \tag{1}$$

while, the primary magnetic vector potential is a free-space Green's function as

$$A_z^p(r,\theta)=\frac{\mu_1 J}{4\pi}\frac{e^{ik_1R}}{R}, \tag{2}$$

$\hat{z}$ and $\hat{r}$ are the unit vectors and $R=\sqrt{r^2+r'^2-2rr'\cos\theta}$. And the secondary magnetic vector potential is

$$A_r^s(r,\theta)=\sum_{n=0}^{\infty}a_n\hat{J}_n(k_1r)P_n(\cos\theta), \tag{3}$$

where $\hat{J}_n(.)$ and $P_n(.)$ are the spherical Bessel and Legendre functions, respectively, and [11]

$$a_n=\frac{\mu_1 aJ}{8\pi k_1\hat{J}_n'(k_1a)}\frac{2n+1}{n(n+1)}\int_0^{\pi}\Omega\frac{\partial P_n(\cos\theta)}{\partial\theta}\sin^2\theta d\theta \tag{4}$$

$$\Omega=\begin{Bmatrix}\left(a^2-2r'^2+ar'\cos\theta\right)\left(ik_1\tilde{R}-1\right)\\ +k_1^2\tilde{R}^2\left(a^2-ar'\cos\theta\right)\end{Bmatrix}\frac{e^{ik_1\tilde{R}}}{\tilde{R}^5}.$$

Now consider a slotted conducting sphere, as shown in Fig. 1a. The total magnetic vector potential in region (I) consists of the incident A^i and scattered A_r^I potentials as

$$A_r^I(r,\theta)=\sum_{n=0}^{\infty}C_n\hat{J}_n(k_Ir)P_n(\cos\theta). \tag{5}$$

Here, C_n is an unknown modal coefficient. The r-component of the magnetic vector potential in region (II, III, IV, and V) of the l-th slot is

$$A_r^{\gamma}(r,\theta)=\sum_{v=0}^{\infty}R_v^{l,\gamma}(\cos\theta)\left[D_v^{l,\gamma}\hat{J}_{\xi_v^l}(k_\gamma r)+E_v^{l,\gamma}\hat{N}_{\xi_v^l}(k_\gamma r)\right], \tag{6}$$

where $\gamma=II,III,IV,V$ and

$$R_v^{l,\gamma}(\cos\theta)=\begin{cases}Q_{\xi_v^l}(\cos\theta) & v=0\\ Q_{\xi_v^l}(\cos\alpha_2^l)P_{\xi_v^l}(\cos\theta)- \\ P_{\xi_v^l}(\cos\alpha_2^l)Q_{\xi_v^l}(\cos\theta) & v\geq 1\\ P_{\xi_v^l}(\cos\theta)+G_{\xi_v^l}^{\gamma}Q_{\xi_v^l}(\cos\theta) & III,IV\end{cases} \tag{7}$$

The r-component of the magnetic vector potential in region (VI) is

$$A_r^{VI}(r,\theta)=\sum_{v=0}^{\infty}F_n\hat{H}_n^{(2)}(k_{VI}r)P_n(\cos\theta), \tag{8}$$

where F_n is an unknown modal coefficient and $\hat{H}_n^{(2)}(.)$ is the spherical Hankel function of the second kind.

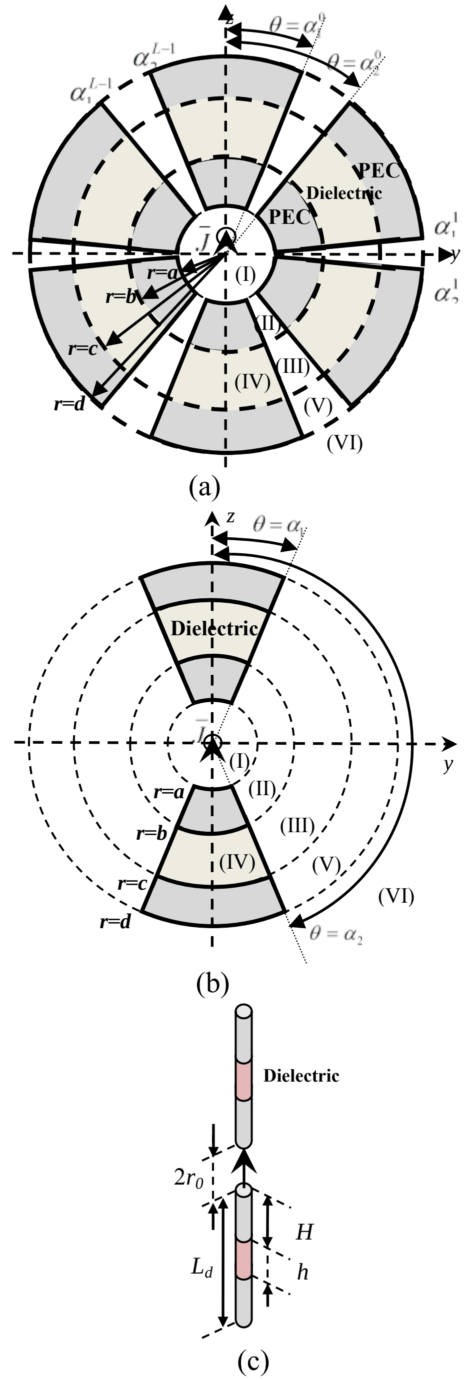

Fig. 1. (a) Multiply- (b) single slotted dielectric loaded conducting hollow sphere, and (c) dielectric loaded dipole antenna: cross-sectional view, a=0.1mm, b=2.5mm, h=|c-b|=0.5mm, d=5mm, r_0=0.1mm, H=2.4mm, L_d=4.9mm, and the dipole radius, r_d, is equal to 0.1mm.

To determine the modal coefficients, we enforce the field continuities as Table 1.

Table 1: Boundary conditions

Layer	Electric Field	Magnetic Field	Limit
I,II	$E_\theta^{II}=\begin{cases}E_\theta^{I} & \alpha_1^q<\theta<\alpha_2^q\\ 0 & otherwise\end{cases}$	$H_\varphi^{i}+H_\varphi^{I}=H_\varphi^{II}$	$r=a$
II, III	$E_\theta^{III}=\begin{cases}E_\theta^{II} & \alpha_1^q<\theta<\alpha_2^q\\ 0 & otherwise\end{cases}$	$H_\varphi^{III}=H_\varphi^{II}$	$r=b$
III, V	$E_\theta^{III}=\begin{cases}E_\theta^{V} & \alpha_1^q<\theta<\alpha_2^q\\ 0 & otherwise\end{cases}$	$H_\varphi^{III}=H_\varphi^{V}$	$r=c$
VI, V	$E_\theta^{VI}=\begin{cases}E_\theta^{V} & \alpha_1^q<\theta<\alpha_2^q\\ 0 & otherwise\end{cases}$	$H_\varphi^{VI}=H_\varphi^{V}$	$r=d$
III, IV	$E_r^{IV}=E_r^{III}$	$H_\varphi^{VI}=H_\varphi^{III}$	$b<r<c$, $\theta=\alpha_{1,2}^q$

Applying orthogonal integrals and mathematical manipulation some can write the equations as follow, [18]

$$C_n=-\sqrt{\frac{\mu_I\varepsilon_I}{\mu_{II}\varepsilon_{II}}}\frac{2n+1}{2n(n+1)}\frac{1}{\hat{J}_n'(k_I a)}\sum_{l=0}^{L-1}\sum_{v=0}^{\infty}\left[D_v^{l,II}\hat{J}_{\xi_v^l}'(k_{II}a)+E_v^{l,II}\hat{N}_{\xi_v^l}'(k_{II}a)\right]I_{vn}^{l,II}, \tag{9}$$

$$\sum_{l=0}^{L-1}\sum_{v=0}^{\infty}\left\{\begin{aligned}&D_v^{l,II}\left[\hat{J}_{\xi_v^l}'(k_{II}a)X_{uv}^{ql}-\hat{J}_{\xi_v^l}(k_{II}a)K_v^{l,II}\delta_{ql}\delta_{uv}\right]\\&+E_v^{l,II}\left[\hat{N}_{\xi_v^l}'(k_{II}a)X_{uv}^{ql}-\hat{N}_{\xi_v^l}(k_{II}a)K_v^{l,II}\delta_{ql}\delta_{uv}\right]\end{aligned}\right\}=-\frac{\mu_{II}Ja^2}{4\pi}L_u^q+\frac{\mu_{II}}{\mu_I}\sum_{n=0}^{\infty}a_n\hat{J}_n(k_I a)I_{un}^{q,II}, \tag{10}$$

$$\sum_{l=0}^{L-1}\sum_{v=0}^{\infty}\left[D_v^{l,\gamma}\hat{J}_{\xi_v^l}'(k_\gamma r)+E_v^{l,\gamma}\hat{N}_{\xi_v^l}'(k_\gamma r)\right]K_v^{l,\gamma}=\sqrt{\frac{\mu_\gamma\varepsilon_\gamma}{\mu_{\gamma'}\varepsilon_{\gamma'}}}\sum_{l=0}^{L-1}\sum_{v'=0}^{\infty}\left[\begin{aligned}&D_{v'}^{l,\gamma'}\hat{J}_{\xi_{v'}^l}'(k_{\gamma'}r)\\&+E_{v'}^{l,\gamma'}\hat{N}_{\xi_{v'}^l}'(k_{\gamma'}r)\end{aligned}\right]K_{v'}^{l,\gamma\gamma'}, \tag{11}$$

$$\sum_{l=0}^{L-1}\sum_{v=0}^{\infty}\left[D_v^{l,\gamma}\hat{J}_{\xi_v^l}(k_\gamma r)+E_v^{l,\gamma}\hat{N}_{\xi_v^l}(k_\gamma r)\right]K_v^{l,\gamma}=\frac{\mu_\gamma}{\mu_{\gamma'}}\sum_{l=0}^{L-1}\sum_{v'=0}^{\infty}\left[\begin{aligned}&D_{v'}^{l,\gamma'}\hat{J}_{\xi_{v'}^l}(k_{\gamma'}r)\\&+E_{v'}^{l,\gamma'}\hat{N}_{\xi_{v'}^l}(k_{\gamma'}r)\end{aligned}\right]K_{v'}^{l,\gamma\gamma'}, \tag{12}$$

$$\sum_{v=0}^{\infty}\xi_v^l\left(\xi_v^l+1\right)\left[\begin{aligned}&D_v^{l,III}U_v\\&+E_v^{l,III}U_{vw}\end{aligned}\right]R_v^{l,III}(\cos\theta_0)=\frac{\mu_{III}\varepsilon_{III}}{\mu_{IV}\varepsilon_{IV}}\sum_{v'=0}^{\infty}\xi_{v'}^l\left(\xi_{v'}^l+1\right)\left[\begin{aligned}&D_{v'}^{l,IV}U_{v'v}\\&+E_{v'}^{l,IV}U_{v'w}\end{aligned}\right]R_{v'}^{l,IV}(\cos\theta_0), \tag{13}$$

$$\sum_{l=0}^{L-1}\sum_{v=0}^{\infty}\left\{\begin{aligned}&D_v^{l,V}\left[\hat{J}_{\xi_v^l}'(k_V d)\Psi_{uv}^{ql}-\hat{J}_{\xi_v^l}(k_V d)K_v^{l,V}\delta_{ql}\delta_{uv}\right]\\&+E_v^{l,V}\left[\hat{N}_{\xi_v^l}'(k_V d)\Psi_{uv}^{ql}-\hat{N}_{\xi_v^l}(k_V d)K_v^{l,V}\delta_{ql}\delta_{uv}\right]\end{aligned}\right\}=0, \tag{14}$$

$$F_n=-\sqrt{\frac{\mu_{VI}\varepsilon_{VI}}{\mu_V\varepsilon_V}}\frac{2n+1}{2n(n+1)}\frac{1}{\hat{H}_n'^{(1)}(k_{VI}d)}\sum_{l=0}^{L-1}\sum_{v=0}^{\infty}\left[D_v^{l,V}\hat{J}_{\xi_v^l}'(k_V d)+E_v^{l,V}\hat{N}_{\xi_v^l}'(k_V d)\right]I_{vn}^{l,V}, \tag{15}$$

where $\gamma=II,V,\ \gamma'=III,\ r=b,c,\ and\ \theta_0=\alpha_1^l,\alpha_2^l$.

The required definitions are illustrated in the appendix. For a single slot configuration (biconical antenna loaded with a dielectric, Fig.1-b), due to the magnetic field boundary condition between region III and IV, $R_v^{l,\gamma}(\cos\theta)$ has been simplified as

$$R_v^{l,\gamma}(\cos\theta)=\begin{cases}\begin{cases}Q_{\xi_v^l}(\cos\theta) & v=0\\ Q_{\xi_v^l}(\cos\alpha_2)P_{\xi_v^l}(\cos\theta)-P_{\xi_v^l}(\cos\alpha_2)Q_{\xi_v^l}(\cos\theta) & v\ge 1\end{cases} & II,V\\ P_{\xi_v^l}(\cos\theta)+\left(\frac{\mu_{III}}{\mu_{IV}}-1\right)\left[\frac{P'_{\xi_v^l}(\cos\alpha_1)-P'_{\xi_v^l}(\cos\alpha_2)}{Q'_{\xi_v^l}(\cos\alpha_1)-Q'_{\xi_v^l}(\cos\alpha_2)}\right]Q_{\xi_v^l}(\cos\theta) & III\\ P_{\xi_v^l}(\cos\theta) & IV\end{cases}. \tag{16}$$

Finally, the unknown coefficients are

$C_n,\ D_v^{II},\ E_v^{II},\ D_v^{III},\ E_v^{III},\ D_v^{IV},\ E_v^{IV},\ D_v^{V},\ E_v^{V},\ F_n$.

III. NUMERICAL ANALYSIS

From the formulas presented in the previous section, it is straightforward to write short programs that illustrate the difference between the different types of material inclusions. To this aim, the cone angle of the biconical antenna is selected to be as small as possible, e.g., $2\alpha_1$=2.5 degree. It should be noted that, based on [12-13], it is well known that the input impedance of a biconical antenna changes significantly by changing cone angle. Hence the input impedance of a biconical antenna is investigated with regards to its cone angle. The inverse radiation impedance Z_v for biconical antennas is given by [11]

$$Z_v=\frac{j\eta_2\sin\alpha_1\ln\left(\cot\frac{\alpha_1}{2}\right)\sum_{v=0}^{\infty}\left[\begin{aligned}&D_v^{II}\hat{J}_{\xi_v}(k_{II}b)\\&+E_v^{II}\hat{N}_{\xi_v}(k_{II}b)\end{aligned}\right]\left.\frac{\partial R_{\xi_v}(\cos\theta)}{\partial\theta}\right|_{\theta=\alpha_1}}{\pi\left[D_0^{II}\hat{J}_0'(k_{II}b)+E_0^{II}\hat{N}_0'(k_{II}b)\right]}. \tag{17}$$

The analytic simulations have been compared with the CST simulation results of an equivalent dipole antenna (radius, r_d). The results have been presented in Fig. 2. According to this figure, for the antenna radius r_d <0.01λ (≈biconical antenna $2\alpha_1$≤3.4 degree, with regards to f=25GHz as main frequency) the loaded dipole may be considered as a limit case of a loaded biconical antenna (the approximation meet numerical simulations with good agreement). The simulation parameters are: a=0.1mm, b=2.5mm, h=0.5mm, d=5mm, r_0=0.1mm, H=2.4mm, L_d=4.9mm, ε_r=2.2, and μ_r=1. For the radius $0.01\lambda<r_d<0.02\lambda$, the antenna input impedance has been extracted approximately, and larger values cause significant errors in impedance computations.

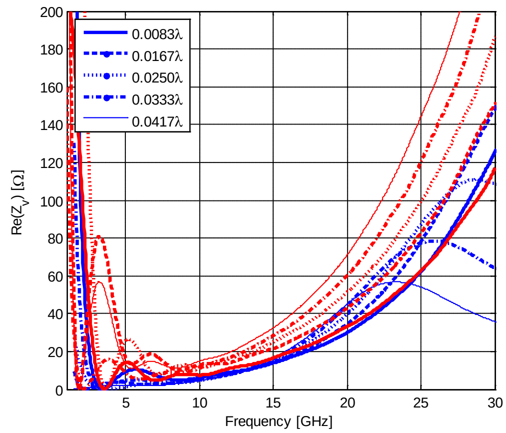

(a)

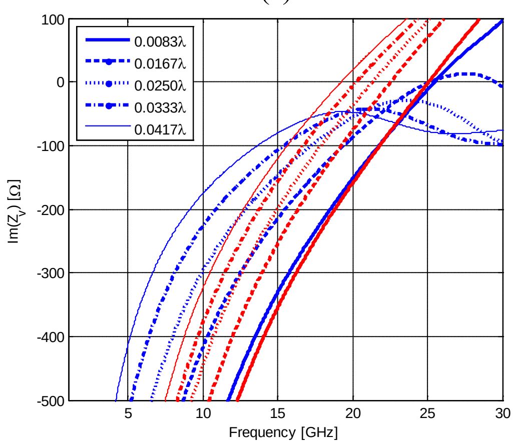

(b)

Fig. 2. Input impedance of a DPS-loaded dipole v.s. dipole radius, (a) real, and (b) imaginary parts: analytical (Blue) against numerical results (Red). Analytical results are obtained using proposed analytical expressions; while the numerical results are extracted using CST software.

A. Dielectric-covered biconical antennas

To validate the proposed method, it is useful to consider a conventional covered biconical antenna (Fig. 3) as the first limiting case. The input impedance of a thin biconical antenna embedded in dielectric material has been derived by Tai [14]. A slightly more general expression applicable to a biconical antenna embedded in a lossless material of arbitrary permeability and permittivity has been given by [15]. Assuming $L=1$, the region III fills by PEC, and $k_1 a << 1$; the slotted sphere becomes a simple biconical antenna, (Fig. 3). In Fig. 4, the effects of the numbers of modes in computation convergence have been depicted. It is clear that good convergence has been achieved.

In Fig. 5, the analytic results for the return loss of a biconical antenna have been compared with CST simulation results. As it is stated before, the antenna cone angle is $2\alpha_1$=2.5 degree. According to this figure, a good agreement has been achieved between analytic and numeric simulations.

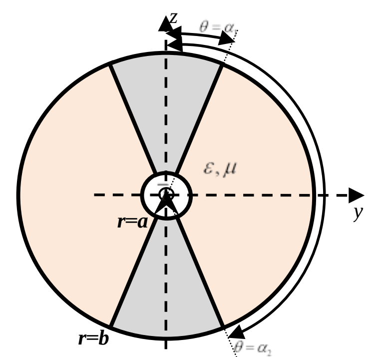

Fig. 3. Dielectric-covered biconical antenna: cross-sectional view, a=0.1mm, b=5mm, ε_r= μ_r =1.

B. Dielectric-loaded biconical antennas

In order to demonstrate the capability of the MTM loading to realize a miniaturized antenna, two examples are studied here. The first one is a dipole antenna filled with double positive (DPS) material inclusions, (ε_r=2.2 and μ_r=1). A DNG-loaded dipole antenna, whose parameters are labeled in Fig. 1-c, is also studied.

Here, the Drude model [16] is used to simulate the MTM inclusions, since it can yield a negative real part of the permittivity/permeability over a wide frequency range. For the DNG inclusions, both μ and ε obey the Drude model (with plasma frequency ω_p=15×10^{10} rad/s and collision frequency f_c =0.01GHz) as

$$\xi_r(\omega)=\xi_\infty-\frac{\omega_p^2}{\omega(\omega-iv_c)} \quad \xi\in\{\varepsilon,\mu\}. \tag{18}$$

It should be noted that, this selection has been affected by all the other relative parameters, e.g., *k*, [17]. In Fig. 6, the effects of the numbers of modes in computation convergence have been presented. Again, it is clear that good convergence has been obtained. The analytical and simulated results for the reflection coefficient of the DPS- and DNG-loaded dipole antennas are presented in Fig. 7. As can be seen from this figure, the analytical results for the reflection coefficient of a loaded dipole are in good agreement with the CST simulation results. Simulations show that for the dipole antenna loaded with DNG-inclusions, an additional resonance frequency is introduced at the frequencies lower than the antenna resonant frequency where the antenna radiates an omnidirectional radiation pattern.

In contrast, for the dipoles loaded with DPS-inclusions, changing DPS locations on the antenna arms causes no resonances at frequencies lower than the main resonant frequency. An important advantage of the proposed antenna is that the dipole length does not need to be increased to lower the resonant frequency. Consequently, a compact antenna is obtained. The proposed method, suggested a bandwidth of 0.3% at 2.2GHz (which is wider than the bandwidth of other miniaturized MTM loaded dipoles [1-2]) while it means 11.8 times frequency reduction with regards to resonance frequency of DPS loaded antenna (26GHz). Since changing the locations and dimensions of the DPS/DNG materials does not have any significant effect on the antenna radiation patterns, the proposed antennas radiate omnidirectional radiation patterns at all resonant frequencies. However, these are not plotted here for the sake of brevity.

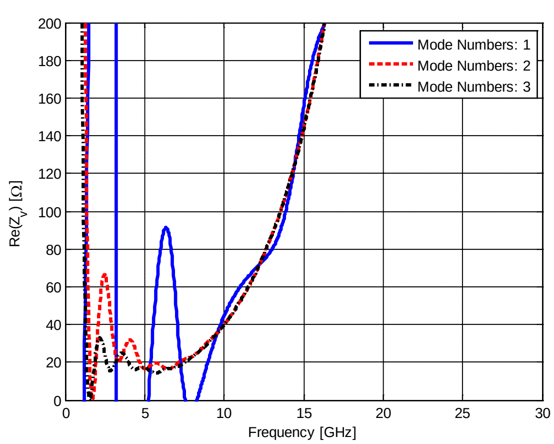

(a)

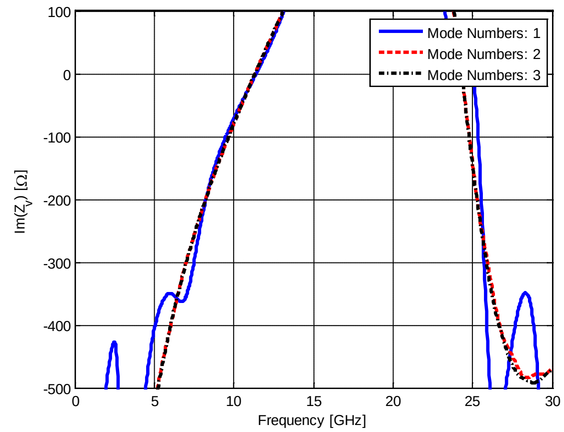

(b)

Fig. 4. Convergence analysis of the dielectric-covered biconical antenna, input impedance, (a) real, and (b) imaginary parts.

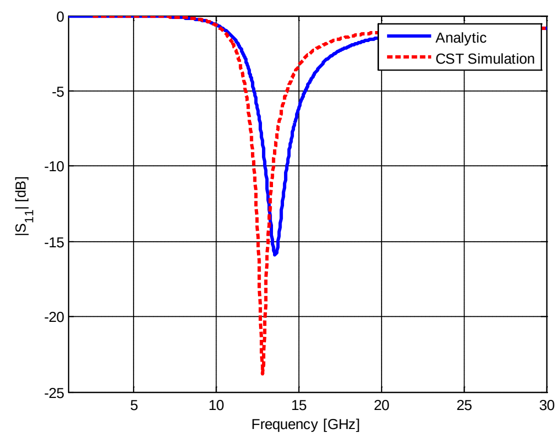

Fig. 5. $|S_{11}|$ [dB] of a dielectric-covered biconical antenna: analytical against numerical results. Analytical results are obtained using proposed analytical expressions; numerical results are computed by CST software.

IV. CONCLUSION

The behavior of a biconical/dipole antenna loaded with MTM inclusions has been examined both analytically and numerically. The theory is compared with different simulation results resulting in a very good agreement between them. The analytical investigations also reveal that embedding DNG-inclusions in a simple biconical/dipole antenna can provide an opportunity to design miniaturized antenna.

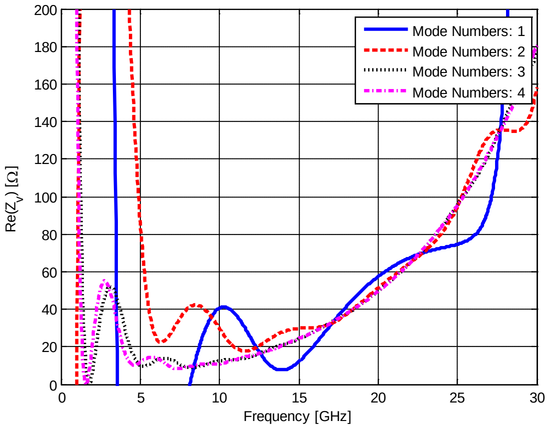

(a)

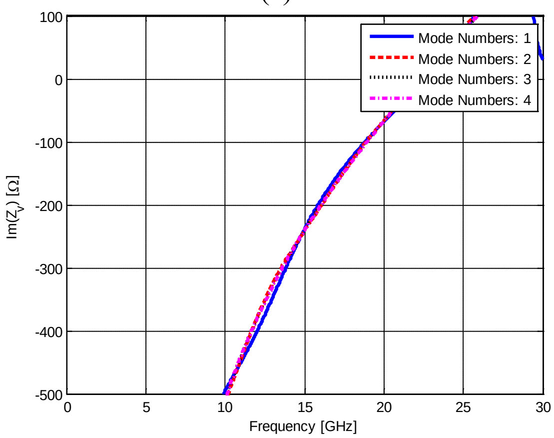

(b)

Fig. 6. Convergence analysis of the dielectric-loaded biconical antenna, input impedance (a) real, and (b) imaginary parts.

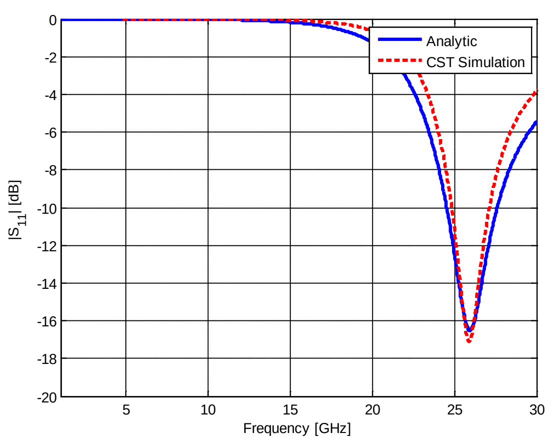

(a)

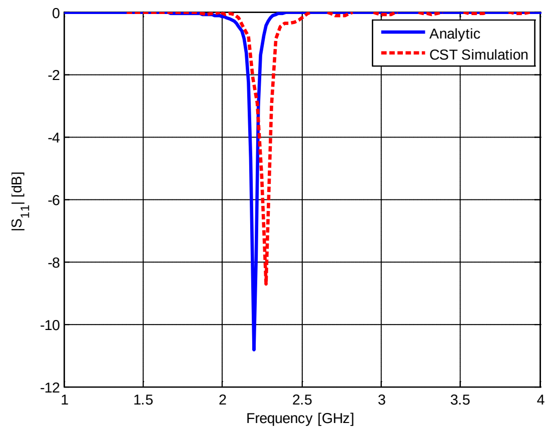

(b)

Fig. 7. $|S_{11}|$ [dB] of a (a) dielectric, and (b) DNG-loaded biconical antenna: analytical against numerical results. Analytical results are obtained using proposed analytical expressions; numerical results are computed by CST software.

ACKNOWLEDGMENT

The authors would like to thank Iran Telecommunication Research Centre (ITRC) for its financial supports.

APPENDIX

In Eqs. (9)-(15) the required definitions are defined as follow:

$$I_{vn} = -\int_{\alpha_1}^{\alpha_2} \frac{\partial}{\partial\theta} R_v(\cos\theta) \frac{\partial}{\partial\theta} P_n(\cos\theta)\sin\theta d\theta, \quad \text{(A-1)}$$

$$X_{uv}^{ql} = \sqrt{\frac{\mu_{II}\varepsilon_I}{\mu_I\varepsilon_{II}}} \sum_{n=1}^{\infty} \frac{2n+1}{2n(n+1)} \frac{\hat{J}_n(k_I a)}{\hat{J}_n'(k_I a)} I_{un}^{q,II} I_{vn}^{l,II}, \quad \text{(A-2)}$$

$$L_u^q = \int_{\alpha_1^l}^{\alpha_2^l} \frac{\partial}{\partial\theta}\left(\frac{e^{ik_I R}}{R}\right) \frac{\partial R_u^q(\cos\theta)}{\partial\theta} \sin\theta d\theta, \quad \text{(A-3)}$$

$$K_v^{l,\gamma} = \int_{\alpha_1^l}^{\alpha_2^l} \frac{\partial}{\partial\theta} R_v^{l,\gamma}(\cos\theta) \frac{\partial}{\partial\theta} R_{v'}^{l,\gamma}(\cos\theta)\sin\theta d\theta, \quad \gamma = II, V \quad \text{(A-4)}$$

$$= \begin{cases} Q_0(\cos\alpha_2^l) - Q_0(\cos\alpha_1^l) & v = 0 \\ \xi_v^l(\xi_v^l + 1)\int_{\alpha_1^l}^{\alpha_2^l}\left[R_v^{l,\gamma}(\cos\theta)\right]^2 \sin\theta d\theta & v \ge 1 \end{cases}, \gamma = II, V,$$

$$K_v^{l,\gamma\gamma'} = \int_{\alpha_1^l}^{\alpha_2^l} \frac{\partial}{\partial\theta} R_v^{l,\gamma}(\cos\theta) \frac{\partial}{\partial\theta} R_{v'}^{l,\gamma'}(\cos\theta)\sin\theta d\theta, \begin{matrix} \gamma = II, V \\ \gamma' = III \end{matrix}, \quad \text{(A-5)}$$

$$\Psi_{uv}^{ql} = \sqrt{\frac{\mu_V\varepsilon_{VI}}{\mu_{VI}\varepsilon_V}} \sum_{n=1}^{\infty} \frac{2n+1}{2n(n+1)} \frac{\hat{H}_n^{(2)}(k_{VI} d)}{\hat{H}_n'^{(2)}(k_{VI} d)} I_{un}^{q,V} I_{vn}^{l,V}. \quad \text{(A-6)}$$

REFERENCES

[1] Q. Liu, P. S. Hall, and A. L. Borja, “Efficiency of electrically small dipole antennas loaded with

left-handed transmission lines," *IEEE Trans. Antennas Propag.*, vol. 57, no. 10, pp. 3009-3017, 2009.

[2] H. Iizuka and P. S. Hall, "Left-handed dipole antennas and their implementations," *IEEE Trans. Antennas Propag.*, vol. 55, no. 5, pp. 1246-1253, 2007.

[3] A. Jafargholi, M. Kamyab, and M. Veysi, "Artificial magnetic conductor loaded monopole antenna" *IEEE Antennas Wireless Propag. Lett.*, vol. 9, pp. 211-214, 2010.

[4] A. Jafargholi, M. Kamyab, M. Rafaei, M. Veysi, "A compact dual-band printed dipole antenna loaded with CLL-based metamaterials", *International Review of Electrical Engineering*, vol. 5, no. 6, pp. 2710-2714, 2010.

[5] M. Rafaei Booket, M. Kamyab, A. Jafargholi, and S. M. Mousavi, "Analytical modeling of the printed dipole antenna loaded with CRLH structures," *Progress In Electromagnetics Research B*, vol. 20, pp. 167-186, 2010.

[6] K. M. Z. Shams and M. Ali, "Analyses of a Dipole Antenna Loaded by a Cylindrical Shell of Double Negative (DNG) Metamaterial, "*International Journal of Antennas and Propagation*, Article ID 97481, 10 pages, 2007.

[7] R. Beggs, J. Luebbers, and K. Chamberlin, "Finite difference time-domain calculation of transients in antennas with nonlinear loads," *IEEE Trans. Antennas Propag*., vol. 41, no. 5, p. 566, May 1993.

[8] T. F. Kennedy, K. D. Fasenfest, S. A. Long and J. T. Williams, "Modification and Control of Currents on Electrically Large Wire Structures Using Composite Dielectric Bead Elements, "*IEEE Trans. Antennas Propag*., vol. 54, no. 12, pp. 3608–3613, 2006.

[9] J. D. Kraus, and R. J. Marhefka, *Antennas for All Applications*, McGraw-Hill, 2002.

[10] R. E. Collin, and F. J. Zucker, *Antenna Theory*, McGraw-Hill, 1969.

[11] J. S. Ock, and H. J. Eom, "Radiation of a Hertzian Dipole in a Slotted Conducting Sphere," *IEEE Trans. Antennas Propagat*., vol. 57, no. 12, pp. 3847–3851, 2009.

[12] R. W. king and G. S. Smith, *Antenna in Matter, Fundamentals, Theory, and Applications*, MIT Press, 1981.

[13] S. Saoudy and M. Hamid, "Input Admittance of a Biconical Antenna with Wide Feed Gap," *IEEE Trans. Antennas Propag*., vol. 38, no. 11, pp. 1784–1790, 1990.

[14] C. T. Tai, "On the theon; of biconical antennas," *J. of Appl. Phys*., vol. 19, pp. 1155-1160, 1958.

[15] C. Polk, "Resonance and Supergain Effects in Small Ferromagnetically or Dielectrically Loaded Biconical Antennas, "*IRE Trans. Antennas Propag*., pp. 414-423, 1959.

[16] M. Rafaei Booket, A. Jafargholi, M. Kamyab, H. Eskandari, M. Veysi, and S. M. Mousavi, "A Compact Multi-Band Printed Dipole Antenna Loaded with Single-Cell MTM," pending publication in *IET Microwave Antenna Propag*., 2011.

[17] N. Engheta and R. Ziolkowski, *Metamaterials: Physics and Engineering Explorations*, Wiley, 2006.

[18] A. Jafargholi, and M. Kamyab, *Metamaterials in Antenna Engineering, Theory and Applications*, LAP Lambert Academic Publishing, Germany, 2011.

Amir Jafargholi received the Ph.D. degree in Electrical Engineering from K.N. Toosi University of Technology, Tehran, Iran, in 2011. He is the coauthor of about 50 scientific contributions published in international books, journals and peer-reviewed conference proceedings. His research interest includes the applications of metamaterials in the analysis and synthesis of antennas. Dr. Jafargholi was a recipient of a Student's Best Thesis National Festival award for his BS thesis, on May 2006. He was a recipient of the 22th Khawarizmi International and 13th Khawarizmi Youth Award on Jan. 2009 and Oct. 2011, respectively. He was also the recipient of Research Grant Awarded in Metamaterial 2010.

Manouchehr Kamyab received the B.S. and M.S. from the University of Tehran, Tehran, Iran, and the PhD degree from Michigan State University, in 1982, in Electrical Engineering. His research interest includes the metamaterials and their applications in antenna engineering, electrically small antennas, microwave and millimeter-wave circuits, and mobile communication systems. He is currently an associate professor in the Department of Electrical Engineering, K.N. Toosi University of Technology, Tehran, Iran. Dr. Kamyab is leading a group of graduate students in the areas of negative-refraction metamaterials and their microwave applications, integrated antennas and components for broad-band wireless telecommunications, novel antenna beam-steering techniques, millimeter and submillimeter-wave circuits, as well as scattering and inverse scattering problems.